JOURNAL OF MATERIALS SCIENCE 31 (1996) 6137–6144

# Characterization of $YBa_2Cu_3O_{7-\delta}$ thin films deposited by dc magnetron sputtering

YUPU LI*, J. A. KILNER, J. THOMAS, D. LACEY, L. F. COHEN, A. D. CAPLIN, Y. H. LI, F. M. SABA**
*Centre for High Temperature Superconductivity, Imperial College of Science Technology and Medicine, London, SW7 2BP, UK*

P. G. QUINCEY
*National Physical Laboratory, Teddington, Middlesex, TW11 0LW, UK*

R. E. SOMEKH
*Department of Materials Science and Metallurgy, University of Cambridge, Cambridge CB2 3QZ, UK*

C. JEYNES, Z. H. JAFRI
*Department of Electronic and Electrical Engineering, University of Surrey, Guildford, Surrey GU2 5XH, UK*

It was found from plan-view transmission electron microscopy (TEM) observations that *c*-oriented $YBa_2Cu_3O_{7-\delta}$ (YBCO) films on $LaAlO_3$, prepared by the magnetron sputtering technique had a single crystalline-like YBCO matrix, but always contained some precipitates of impurity phases. A large number of highly defective twin boundaries were also observed in all of these epitaxial films. Such highly defective twin boundaries are thought to be flux pinning centres and also paths for the diffusion of water into YBCO films. Therefore the films need to be passivated against attack from humid air.

## 1. Introduction

It has been reported that high quality $YBa_2Cu_3O_{7-\delta}$ (YBCO) films can be prepared by several different techniques. Amongst them, dc sputtering techniques [1, 2] and pulsed laser deposition [3, 4] are the most successful methods due to the simplicity of their design, ease of control, and high reproducibility. Focusing on dc sputtering techniques, inverted cylindrical magnetron sputtering [1] and high-pressure planar dc-sputtering [2, 3] remain powerful and practical tools for producing high quality YBCO films. However, no (TEM) observations were performed by the group who originally reported on the growth of films using the inverted cylindrical magnetron sputtering process [1], and detailed characterization of the microstructures of such YBCO films at the sub-micron scale have also not been reported.

In this paper, *c*-oriented YBCO films prepared by inverted cylindrical magnetron sputtering [1], at optimal deposition conditions, are characterized by different analysis techniques. From plan-view TEM observations it is clear that these epitaxial films contain a large number of highly defective twin boundaries. Splitting and swelling of the microtwins are also observed. Such highly defective twin boundaries are thought to be flux pinning centres and also paths for the diffusion of water. Therefore, a suitable method to passivate these twin boundaries in YBCO films is required.

## 2. Experimental procedure

The sputtering system used at the National Physical Laboratory (NPL), is essentially based on that reported by Xi *et al.*, used for the inverted cylindrical magnetron sputtering technique [1]. The sputtering target is an annular ring of $YBa_2Cu_3O_7$ material. The inside and outside diameters of the ring are 40 mm and 50 mm, respectively, and its height is 25 mm. During sputtering the substrate is held 20 mm above the target. The sputter gun was operated in the dc mode with a current of 0.67A and a voltage of 150V. The sputtering gas pressure was $0.87 \times 10^2$ Pa and was a mixture of 2/3 argon and 1/3 oxygen. The deposition rate of the film was about 300 nm per h.

The substrate was clamped to a resistive heater with a pure copper shim to improve thermal contact.

* Present address: Texas Center for Superconductivity, University of Houston, Houston, Texas 77204-5932, USA.
** Present address: Toshiba Research and Development Centre, Materials and Device Research Laboratory III, 1 Komukai Toshiba-cho, Saiwaiku, Kawasaki, 210 Japan.

0022–2461  

During film deposition, the temperature of the heater block was 840 °C. After deposition the chamber was backfilled to $250 \times 10^2$ Pa of oxygen, and the sample allowed to cool to about 450 °C over 15 min before the heater was switched off. In this paper, we refer to such YBCO films as NPL series films.

The deposited YBCO films were characterized by ac susceptibility (ACS) [4] using an Oxford Instruments 3001 8T Vibrating Sample Magnetometer (VSM) [5]. Plan-view transmission electron microscopy (TEM) and XTEM were performed using a JEOL 2000 FX instrument [6, 7]. Polarised optical microscopy (POM) was performed using a Nikon Epiphot instrument. Scanning electron microscopy (SEM) was performed using a JEOL JSM-T200 or a JEOL JSM-T220 instrument. X-ray Diffraction (XRD) traces were obtained with Cu-$K\alpha$ irradiation using an automated Philips PW1730 diffractometer [6]. Rutherford backscattering (RBS) was obtained with a 1.5 MeV $^4He^+$ beam of 1 mm diameter and secondary ion mass spectroscopy (SIMS) was performed on an Atomika 6500 instrument [8, 9].

## 3. Results and discussion

### 3.1. Reproducibility of $T_c$ and $J_c$ of NPL films

Some $T_c$ (R = 0) values and magnetization $J_c$ data for typical NPL films are tabulated in Table I. As an example we show in Fig. 1 the resistance versus temperature curve (Fig. 1a) and the inductive transition (Fig. 1b) of sample No. 5. In Fig. 1b, the peak of dV/dT infers $T_c$ (R = 0) [4].

It was found that the NPL YBCO films usually had a $T_c$ of 89–90.8 K. Fig. 2 shows the curves of the magnetization $J_c$ versus the applied field at different temperatures of a typical NPL film (No. 5). The applied field is parallel to the *c*-axis of the film to make sure that the supercurrent is flowing in the Cu–O planes (i.e. the *a–b* planes). At 77 K and zero field the $J_c$ is equal to $1.9 \times 10^6$ A cm$^{-2}$, which is about half of the reported highest transport $J_c$ (77 K and 0 T) of epitaxial YBCO films [1–3, 10–12].

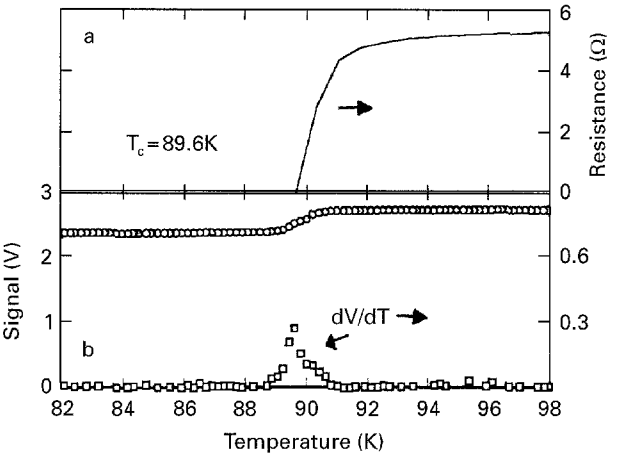


*Figure 1* (a) Resistance versus temperature curve of sample No. 5; (b) The corresponding inductive transition measured from the real part of the magnetic susceptibility.

### 3.2. Microstructure of NPL films

#### *3.2.1. Highly defective twin boundaries in NPL films*

Plan-view TEM images (shown in Fig. 3 (a and c)) and corresponding selected area diffraction (SAD) patterns (shown in Fig. 3 (b and d)) of typical NPL films (Nos 4 and 5) respectively, show that the films are *c*-oriented and contained a large number of microtwin boundaries on the {1 1 0} planes which are separated by 20–90 nm. The presence of microtwins yields spots that are elongated and/or split parallel to the ⟨1 1 0⟩ or ⟨1 $\bar{1}$ 0⟩ direction in the electron diffraction patterns obtained with a parallel ⟨0 0 1⟩ beam (see, for example the SAD patterns in Fig. 3(b and d)). Such microtwins were easily observed in the present plan-view TEM observations, although they appeared to have a non-uniform distribution. The microtwins were formed in order to reduce the strain energy produced by the shape and volume changes associated with the tetragonal to orthorhombic structural phase transformation (TOSPT) during the slow cooling process [13, 14]. Therefore, the most commonly

TABLE I The details of eleven typical samples referred to in the text.

| Sample No. | Device used | Substrate | Thickness (nm)* | $T_c$ (K) | $J_c$ (A cm$^{-2}$)** |
|---|---|---|---|---|---|
| No. 1 | NPL | $LaAlO_3$ | 250 | 90.6 | |
| No. 2 | NPL | $LaAlO_3$ | 200 | 89 | $2.3 \times 10^7$ at 10 K |
| No. 3 | NPL | $LaAlO_3$ | 200 | 90.8 | |
| No. 4 | NPL | $LaAlO_3$ | 100 | 89.6 | $6.8 \times 10^6$ at 10 K |
| | | | | | $5.4 \times 10^6$ at 30 K |
| | | | | | $2.7 \times 10^6$ at 50 K |
| | | | | | $4.6 \times 10^5$ at 77 K |
| No. 5 | NPL | $LaAlO_3$ | 250 | 89.6 | $3.7 \times 10^7$ at 10 K |
| | | | | | $2.3 \times 10^7$ at 30 K |
| | | | | | $1.1 \times 10^7$ at 50 K |
| | | | | | $1.9 \times 10^6$ at 77 K |
| No. 6 | NPL | $LaAlO_3$ | 250 | 89.2 | $1.6 \times 10^7$ at 10 K |
| | | | | | $9.4 \times 10^6$ at 30 K |
| | | | | | $5.1 \times 10^6$ at 50 K |
| | | | | | $1.3 \times 10^6$ at 77 K |

* The thicknesses tabulated here are the nominal thicknesses estimated from the sputtering time and experience, some are corrected by SIMS, RBS, or XTEM analyses without consideration of surface roughness.
** $J_c$ at zero field.

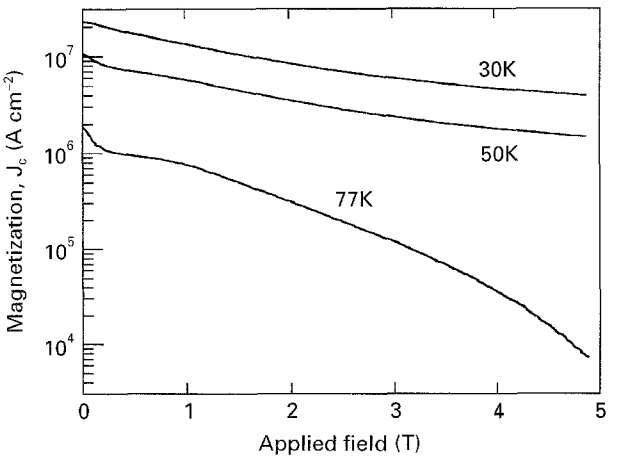


*Figure 2* The magnetization $J_c$ versus the applied field at different temperatures for sample No. 5. The Bean model [25] is used for calculating $J_c$.

observed defects in *c*-oriented YBCO films are twin boundaries [2, 3, 7, 12], which is also the case in the bulk of polycrystalline [15] and single crystal YBCO [16, 17].

Detailed TEM observation of the films at higher magnification shows some details of the twin boundaries. For example, Fig. 4 (a and b) (plan-view TEM images from sample No. 5) clearly show that twin boundaries in the films are frequently bent and contain some steps and dips. It should be noted that Eibl *et al.* reported that twin boundaries in YBCO films prepared by laser ablation contained similar defects [12]. Splitting of the microtwins can be seen in Fig. 4a (see, for example, the label SP in this figure). In some regions swelling of the microtwins can also be seen (see, for example, the label SW in Fig. 4b). No such picture has been reported in bulk YBCO materials. It is clear that the twin boundaries in the films are highly defective, since they have become deformed. The reason for this is probably due to the strain energy from the shape and volume changes resulting from the TOSPT during the cooling process. The YBCO films cannot effectively release this strain through regular twin boundaries which appear as "straight lines" on the conventional TEM image and have a lattice shift across the boundaries in bulk YBCO materials [13, 14]. Compared to YBCO thin films, the strain energy in YBCO bulk materials must be more easily released through regular twin boundaries. Therefore, when comparing twin boundaries within the YBCO films with twin boundaries within bulk YBCO single and polycrystalline materials, two special points need to be considered: i) twin boundaries in YBCO films are highly defective; and ii) in YBCO films, the distance (20–90 nm, averaged as 45 nm) between two twin boundaries is smaller by approximately one order of magnitude compared with bulk polycrystalline YBCO ceramics prepared by a conventional mixed oxide procedure [12, 15]. It is also smaller than bulk YBCO single crystals which have twin domains about 100 nm wide [16]. In addition, only in two films did we see a few dislocations running between two twin boundaries (see, for example, mark d in Fig. 4b), which means that the dislocation density in these films is $\sim 10^6$ per cm$^2$ or less.

### 3.2.2. Epitaxial defects in NPL films

XTEM images show that all films grew with epitaxial defects. See, for example, Fig. 5 (a and b). Interestingly, a decreasing density of such defects is observed in the films with increasing distance from the interface between the film and substrate, as is shown in Fig. 5a, and more clearly in Fig. 5b. In Fig. 5a, the dark region at the bottom of the film, in this conventional (i.e. diffraction-contrast) XTEM image, implies that the bottom of the film grew with more defects than did the upper region of the film. The high resolution XTEM image shown in Fig. 5b clearly shows that the (0 0 *l*) atomic planes are bending and wavy due to frequent faults in the stacking sequence, especially at the bottom of the film. There is a shifted spacing of about 1/2 *c*-axis lattice parameter, some as indicated by arrows. In addition, some small regions (e.g. $<10$ nm) within the *c*-axis layer structure are not resolved (see, for example, the label S in Fig. 5b), which are small precipitates of a second phase. XTEM images also show a clear interface and thus no interaction between the film and the substrate.

### 3.2.3. Precipitates of second phases in NPL films

Precipitates of second phases with different sizes can be observed by plan-view TEM in the NPL films, as is shown in Fig. 3 (a and c). Larger sized second phase precipitates (which form weak-links) can also be seen by POM (not shown) and SEM micrographs (see, for example, Fig. 6b). Some regions of the NPL films show extra spots in addition to those spots of the 123 phase in the SAD patterns (see, for example, mark AS in Fig. 3 (b and d)). Combining the micro-diffraction pattern and energy dispersive X-ray spectroscopy (ED), data from the second phase precipitates, some impurity phases can be identified. For NPL films, $CuO_x$, $BaCu_2O_{2-x}$, and $Y_2O_3$ precipitates [18] and amorphous Y-rich/Cu-poor amorphous islands [17] could be identified. In switching from one sample to another, the type, size, and density of, second phase precipitates could be different. Fig. 7 shows that for the NPL film (No. 2) a better fit between the measured RBS spectrum and simulated structure can be achieved by assuming a structure of $Y_{1.1}Ba_{1.9}Cu_{2.9}O_{6.9}/LaAlO_3$, which can also be represented as $(Y_1Ba_2Cu_3O_{6.9})(Y_2O_3)_{0.065}$ (i.e. an excess of $Y_2O_3$). It is difficult to exactly estimate the volume percentage of precipitates of second phases in the 123 matrix by TEM observations due to their irregular shapes and non-uniform distribution. However, it should be noted that a 5 vol % of second phase precipitates would result in 13.6% of the area in the plan-view TEM image being covered by these precipitates (under the assumption that precipitates of second phases have a cubic shape).

TEM, POM, SEM, and XRD measurements showed that all characterized NPL films (sample size: $\sim 25$ mm $\times$ 25 mm) appeared to be free of any traces of *a*-oriented grains.

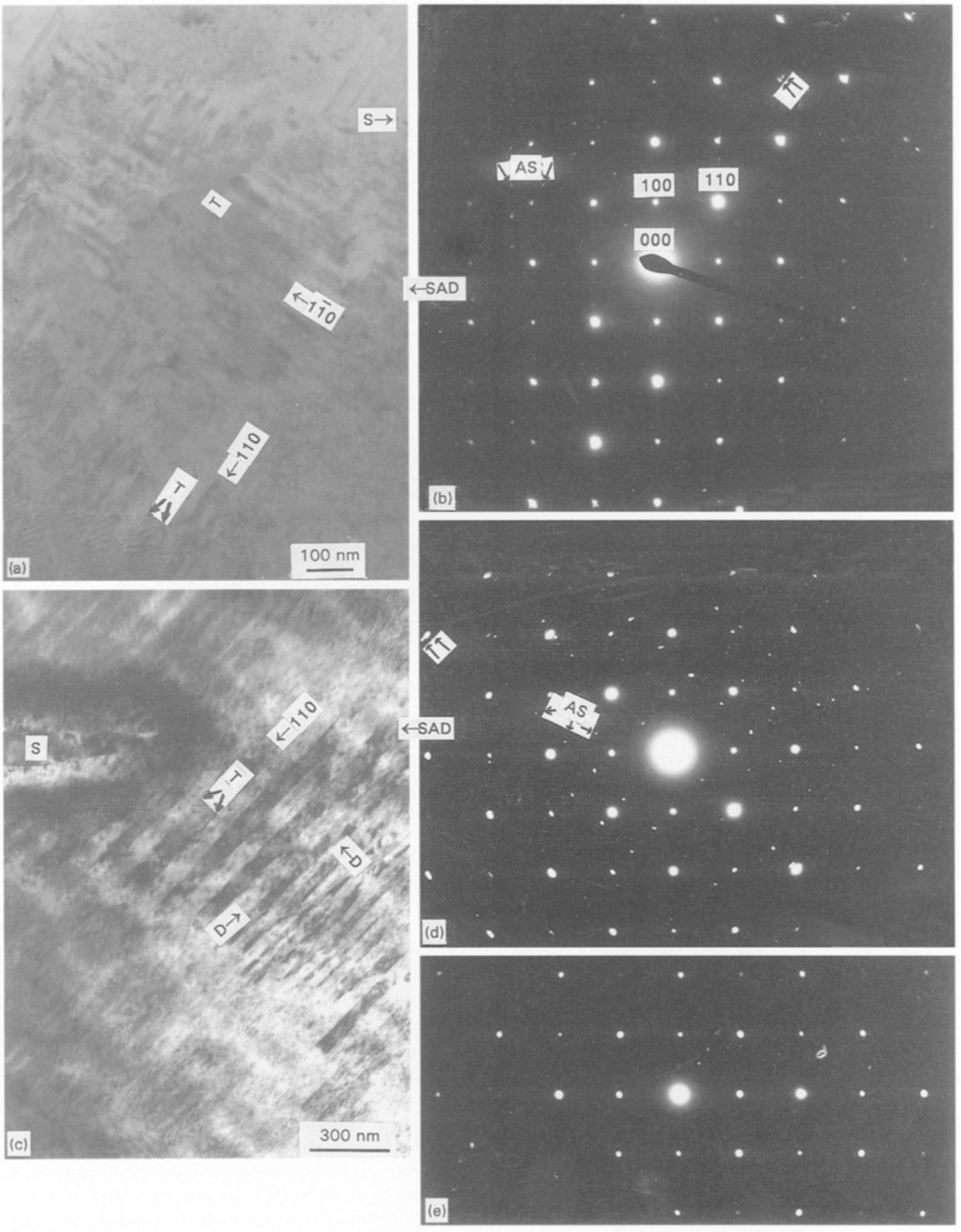


*Figure 3* (a) and (b) Plan-view TEM micrograph and corresponding selected area diffraction (SAD) pattern of sample No. 4; (c) and (d) Plan-view TEM micrograph and corresponding SAD pattern of sample No. 5, (e) SAD pattern from a second smaller region of sample No. 5. It should be noted that all (⟨001⟩ axis) SAD patterns shown in this paper are from an approximately 6 $\mu m^2$ observed area except for (e) which came from a 0.6 $\mu m^2$ observed area. Marks used in this figure: T—twin boundaries; S—precipitates of second phases; D—dips or steps in twin boundaries; and AS—the extra spots from precipitates of second phases.

### 3.3. Possible pinning centres in NPL films

If YBCO films are to carry a large critical current, it is essential that the fluxons should be pinned. The possible role of different kinds of structural defects in high temperature superconductors (such as twin boundaries, the strain field, texture, the small size precipitates of second phases, and dislocations, etc.) as flux pinning centres has been extensively discussed in

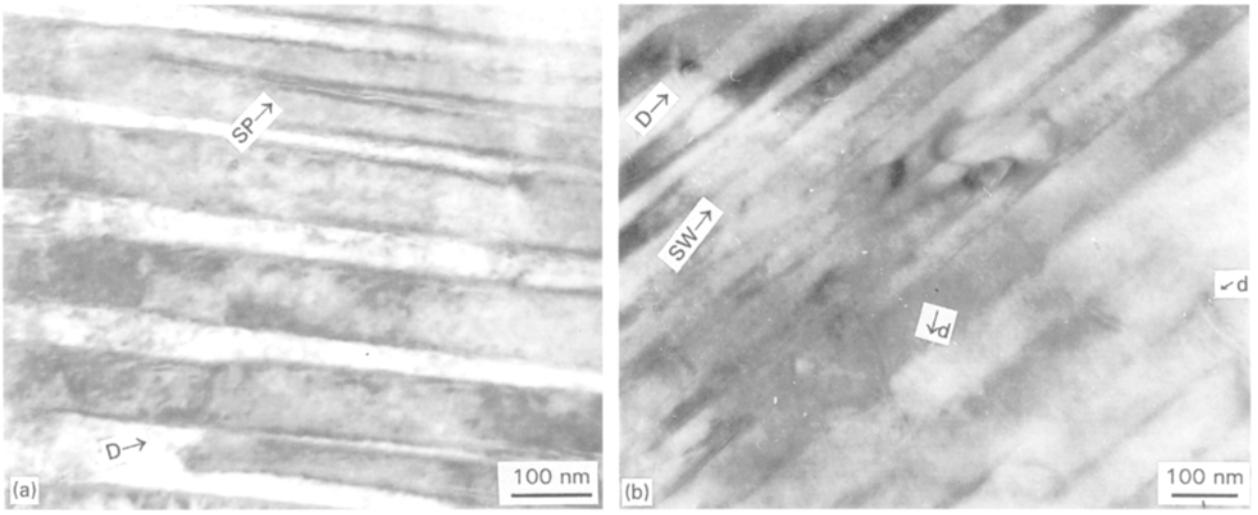


*Figure 4* (a) and (b) Plan-view TEM micrographs of sample No. 5, with the electron beam being along the ⟨001⟩ axis. Marks used in this figure: SP—splitting of the microtwins; SW—swelling of the microtwins; D—dips or steps in twin boundaries; and d—dislocations.

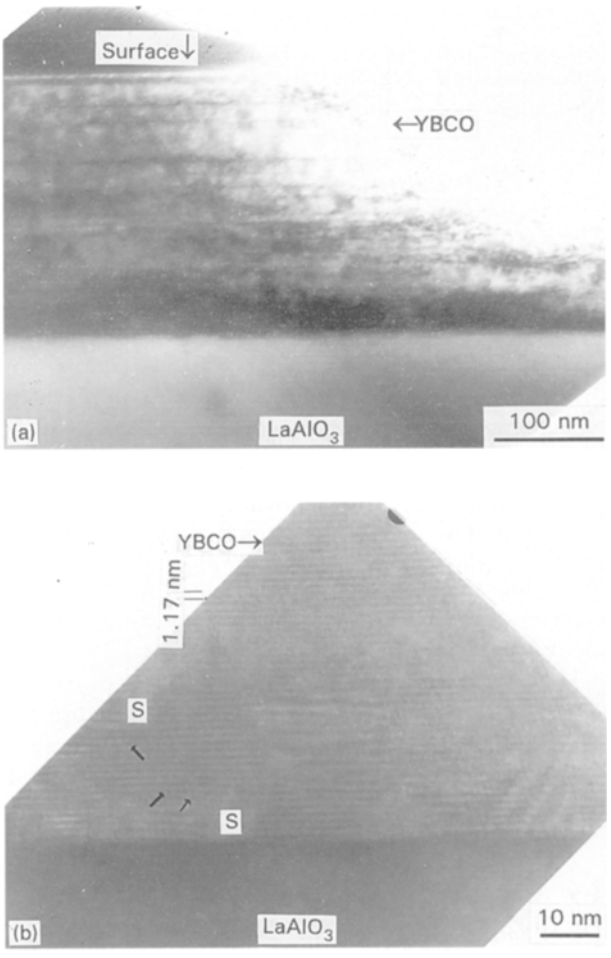


*Figure 5* (a) Conventional XTEM micrograph of sample No. 1 and (b) high-resoultion XTEM image of sample No. 2.

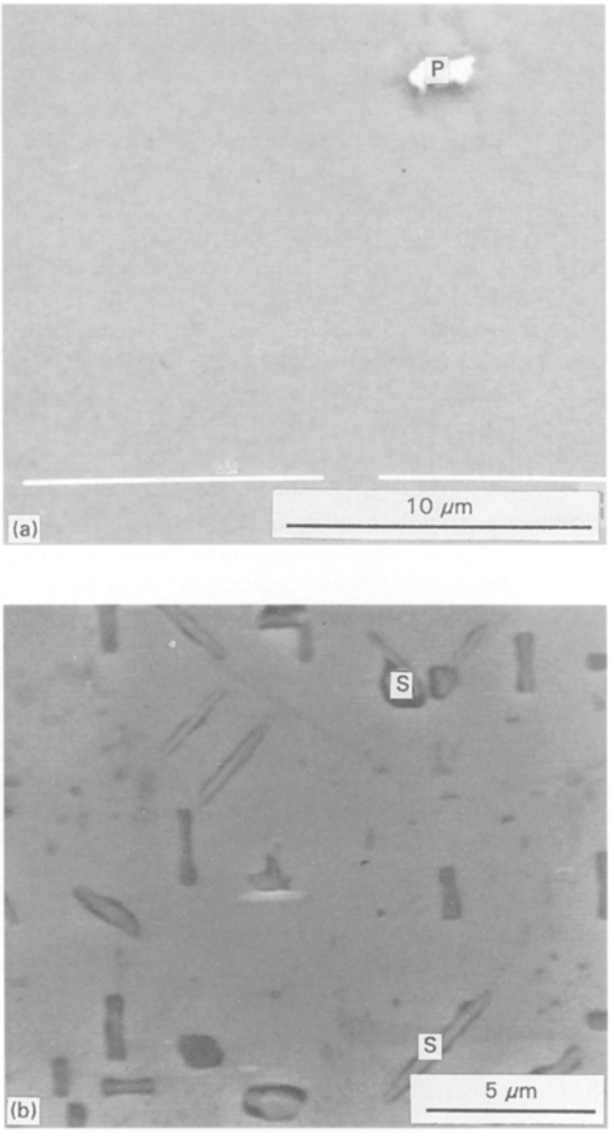


*Figure 6* (a) and (b) SEM micrographs of sample No. 4 and sample No. 5. Marks used in this figure: A—*a*-oriented grains; S—precipitates of second phases; H—pinholes; P—particulates on surface of the film.

the literature. The ideal pinning centres, as they are some kind of structural defects, clearly should be smaller than or at least of the same order of magnitude as the coherence length. At a given temperature (such as 77 K) and field, $\xi_{ab}$ can be estimated to be a few nm [16, 19]. Therefore, for the *c*-oriented films, structural defects with a size of a few nm or smaller could be pinning centres. For the characterized NPL films, these structural defects could be: i) highly defective

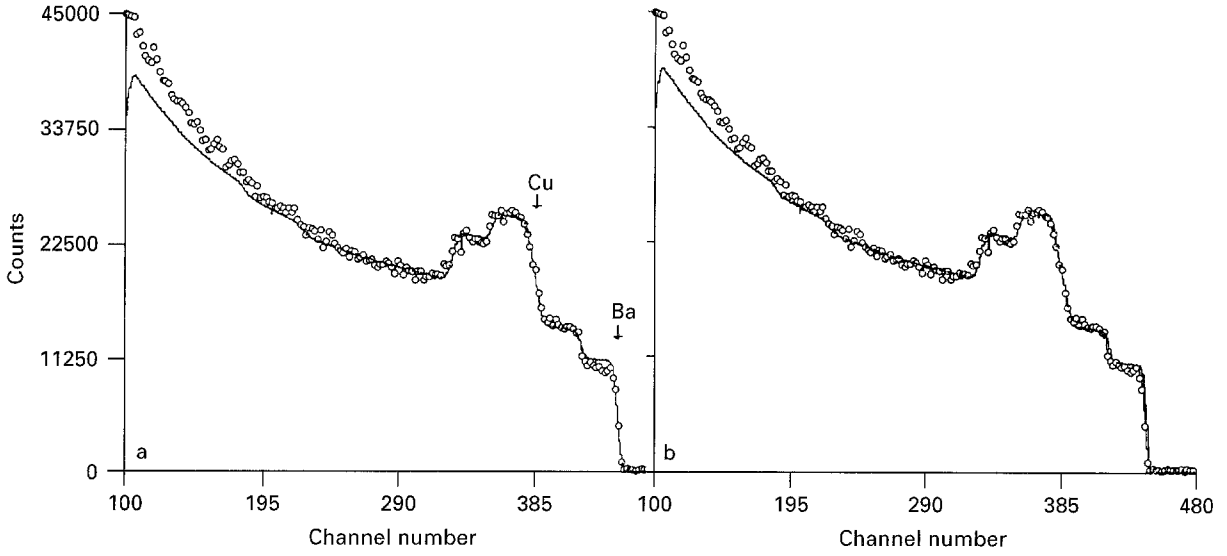


*Figure 7* (a) Rutherford backscattering (RBS) spectrum (opened circles) of sample No. 2. Solid line in this figure is the computer simulated spectrum for $YBa_2Cu_3O_7$ with a density of 6.5 g cm$^{-3}$, (b) Compares the RBS spectrum (opened circles) to a simulated structure $YBa_{1.9}Cu_{2.9}O_{6.9}$ (solid line).

twin boundaries, ii) the local strain field induced by the defective growth of the film, iii) smaller size precipitates of second phases, and iv) dislocations.

### 3.3.1. Highly defective twin boundaries

It should be noted that bulk YBCO single crystals with a much lower $J_c$ ($\sim 10^4$ A cm$^{-2}$ at 77 K and 0 T) are also twinned. Therefore, here, we emphasise that twin boundaries in YBCO films are highly defective and have a higher density. In addition, Eibl *et al.* [12] reported that in high resolution TEM images the twin boundary of a dc-sputtered YBCO film has a thickness of about 1 nm in which there is an intermediate zone filled by non-superconductoring material. If it is the case, such highly defective twin boundaries are ideal flux pinning centres in these epitaxial YBCO films. This may be a reason why in YBCO films the $J_c$ is about two orders of magnitude higher than that in the bulk YBCO single crystals [16, 17].

### 3.3.2. Local strain field

All the characterized films clearly grew with epitaxial defects, especially at the bottom of the film. The local strain field induced by the defective growth has been suggested to act as pinning centres in YBCO films [2, 3].

### 3.3.3. Smaller precipitates of second phases

Such precipitates with dimensions smaller than a few nm (i.e. $\leq \xi_{ab}$) can be seen during the TEM observations (see, for example, Fig. 5b), they could be the pinning centres. However, it is difficult to consider a lot of larger size precipitates of second phases in NPL films as pinning centres although the local strain field around them (see, for example, the strain contrast around the marked second phase in Fig. 2c) may contribute to the pinning mechanisms. Basically, they are weak-link regions which make films more "granular" and so limit $J_c$.

### 3.3.4. Dislocations

These can be considered as ideal pinning centres. However, the dislocations in the NPL films were not easily observed by the present plan-view. TEM observations (in up to $\sim 100\ \mu m^2$ observed area for each film). Only in two films did we see a few dislocations (see, for example, mark d in Fig. 4b), which means that the dislocation density is at a $\sim 10^6$ cm$^{-2}$ level or less. Therefore, we do not think that dislocations make a significant contribution to flux pinning centres. Meanwhile, it illuminates the point that, if we can find a suitable method to increase the dislocations density to the $10^8$ cm$^{-2}$ level, we may achieve a further enhancement in $J_c$ by a notable factor in these NPL films.

Here, we do not discuss at all the effect of oxygen vacancies on the pinning mechanisms, because the studied films are nearly fully oxidised. The effects of oxygen vacancies on $J_c$ and $T_c$ will be discussed in a separate paper.

## 3.4. SIMS depth profiles in NPL films

The SIMS raw data from a 250 nm YBCO on $LaAlO_3$ film (No. 1) after a 10-month ageing period in a desiccator following deposition is shown in Fig. 8. Negative secondary ions at masses 16 ($^{16}O^-$, line a) 17 ($^{17}O^-$ and $^{17}OH^-$, line b), 18 ($^{18}O^-$, line c), 27 ($^{27}Al^-$, line d), and 63 ($^{63}Cu$, line e) from the central 25% of the crater area of 300 $\mu m^2$ were monitored sequentially during the sputtering by the 10 keV $Cs^+$ primary beam [8, 9]. The measurement was terminated at the $LaAlO_3$ substrate. The interface between the film and the substrate can be easily inferred from the steps of the $^{27}Al^-$ and $^{63}Cu^-$ signals [8, 9].

The most interesting result from the SIMS analyses of the as-received YBCO films is that the (OH) signal

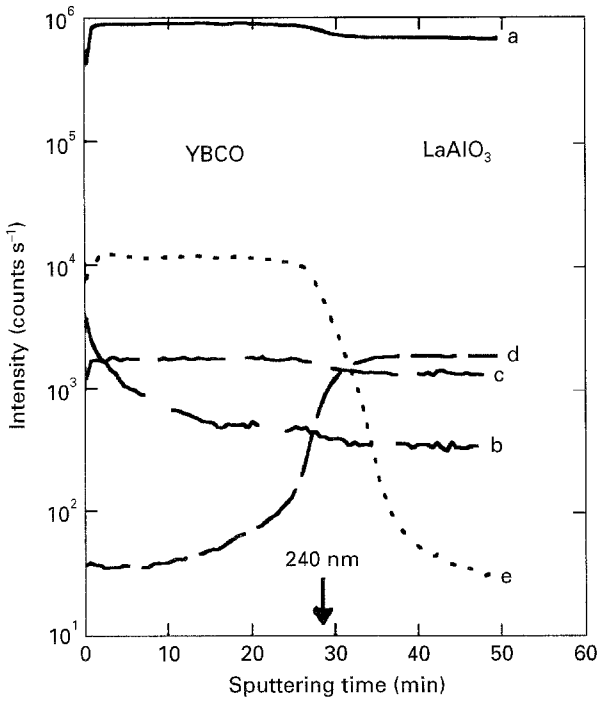


*Figure 8* SIMS raw data of sample No. 1. Line a: $^{16}O^-$; line b: $^{17}Mass^-$ (i.e. $^{17}O^-$ and $^{17}OH^-$); line C: $^{18}O^-$; line d: $^{27}Mass^-$; (i.e. $^{27}Al^-$); line e: $^{63}Mass^-$ (i.e. $^{63}Cu^-$).

shows a declining "diffusion-like" distribution to a depth of about 30–200 nm [6, 8, 9, 20]. For example, in Fig. 8 the measured intensity ratio, i.e. $^{18}Mass^-/[^{16}Mass^- + {}^{18}Mass^-]$, in both the film and the substrate is flat and equal to $\sim 0.2\%$ (the natural $^{18}O$ isotopic ratio). Here, during the calculation of the intensity ratio, the contribution of $^{17}O$ is ignored, because its natural isotopic abundance of 0.04% is only one fifth of that for $^{18}O$. However, it can be seen that the mass 17 signal shows a declining "diffusion-like" distribution before it becomes flat (to the instrumental background level) at a depth of about 150 nm. In the top layer of the as-received film, the mass 17 signal with the background subtracted should be the contribution of $^{17}(^{16}OH)$ signal [20]. The diffusion-depth is dependent on the quality of the films, and how long the films have been stored (aged). We think that water from humid air (or OH due to water molecules dissolved in the surface of the films) can "diffuse" into YBCO films through the highly defective twin boundaries. The storage conditions for the films also play a role in determining the level and "penetration" depth of OH in the films. In normal laboratory conditions, we do not think that bulk chemical reactions with water [21] can happen within the films, but may happen locally.

This phenomenon represents some degradation of the films as even trace OH species in the top surface layer of the films may alter the properties of the YBCO films. The detailed effects of a small amount of (OH) on the electrical properties and microwave properties have not been examined. Our films, with 10-months ageing in a desiccator and a "diffused" OH distribution up to 150 nm depth show a smaller decrease of $T_c$ (usually $<2$ K). This implies that it is important to keep the films in dry conditions. We have also found that the treatment of a 90 K YBCO film in flowing wet $O_2$ gas (i.e. $O_2$ saturated through a 60 °C water bath) at 500 °C for 2 h results in only part of the film remaining as a superconductor with $T_c \sim 44$ K. A large increase in the OH signal in the film during SIMS analysis was also recorded for this film. During practical utilisation, YBCO films must undergo longer ageing and encounter less protected environments (such as liquid water produced by condensation on warm-up from cryogenic conditions) than in a desiccator. It should also be noted that YBCO films normally have a thickness less than 1 μm, therefore the environmental stability of YBCO films is a larger problem than for bulk YBCO single crystals.

It should be re-emphasised that although highly defective twin boundaries in YBCO films are thought to be flux pinning centres, they are also thought to be short circuits for the diffusion of oxygen [22] and water (or OH species) [20]. Therefore, making YBCO films more stable against ageing and more resistant to humid air/$CO_2$ etching is a challenge to materials scientists. In some cases, this task may have equal importance with attempts to further enhance $J_c$ at a higher applied magnetic field in such YBCO films. Here, 700 keV–1 MeV $Ag^+$ implantation at elevated temperatures is proposed as a strategy to (i) passivate twin boundaries and the internal surfaces (between the 123 phase and precipitates of second phases) and (ii) improve the transport properties. Silver is chosen since it has been shown to have some beneficial effects on the environmental stability and transport and microwave transmission properties of YBCO films [23]. It should be noted that ion implantation into YBCO films at room temperature produced only limited improvement in $J_c$ values of the order of a factor 2 [24]. Thus, a higher implantation temperature has to be chosen to ensure that the films do not become granular (i.e. do not produce weak-links) and instead produces extended defects (such as dislocations) which act as flux pinning centres. The high implantation temperature may also result in some implanted $Ag^+$ migrating to twin boundaries and so decorating and passivating these planar defects. In addition, an *in-situ* post-irradiation annealing step in an $O_2$ ambient is also necessary for oxygen enrichment and/or reordering in the films.

### 3.5. Comparison between NPL films and the YBCO films deposited by an adapted high-pressure planar dc-sputtering system

In reference 7, we reported microstructure and transport properties of *c*-oriented YBCO films on $LaAlO_3$, prepared by an adapted high-pressure planar dc-sputtering device [2, 3], at the University of Cambridge (referred as CAM films in this paper).

There are some differences in microstructure between NPL films and CAM films: (i) TEM observations showed that all the CAM films contained some *a*-oriented grains in a non-uniform distribution; (ii) CAM films usually contain less precipitates of second phases than NPL films; and (iii) CAM films

usually have a lower $J_c$ than NPL films. For CAM films on MgO prepared under the same conditions (as reference samples) using XRD measurements [8, 9] the volume percentage of *a*-oriented grains in the *c*-oriented matrix has been found to be about 3–5 vol %. There are two possible explanations for *a*-oriented grains in the CAM films: (a) the original group who reported the high-pressure planar DC-sputtering technique did not mention that *a*-oriented grains could be seen in their *c*-oriented films [8, 9], therefore, we suspect that such *a*-axis oriented grains are due to a narrow heater being used in the Cambridge sputtering device causing a non-uniform surface temperature during the film deposition. A weak thermal contact between the substrate and the heater-plate can produce similar results; (b) using pure $O_2$ in the higher pressure ($2.25 \times 10^2$–$3 \times 10^2$ Pa) as sputtering gas can easily result in such *a*-oriented grains. In addition, *a*-oriented grains within the *c*-oriented matrix in CAM films may be responsible for the lower $J_c$ in the CAM films compared to the NPL films. It is reported that the zero temperature coherence length along the *c*-axis $\xi_c(0)$ and in the *a*–*b* plane $\xi_{ab}(0)$ in the YBCO film are estimated to be 0.22 nm and 1.6 nm [16]. Thus, the supercurrent flowing in the *a*–*b* planes of the *c*-oriented matrix is limited in the *c*-direction of such *a*-oriented grains.

## 4. Summary

Epitaxial thin films of *c*-axis oriented $YBa_2Cu_3O_{7-\delta}$ prepared on (100) $LaAlO_3$ substrates by the inverted cylindrical magnetron sputtering method were characterized by several analytic techniques. In these films the majority of defects are found to be highly defective twin boundaries. Such highly defective twin boundaries are thought to be flux pinning centres and also paths for the diffusion of water, therefore they need to be passivated. $Ag^+$ implantation at elevated temperatures is proposed as a strategy to (i) overcome the effect of these twin boundaries upon factors such as environmental degradation and (ii) improve the transport properties of YBCO films.


## Acknowledgements

This work was funded by the Engineering and Physical Sciences Research Council, United Kingdom. The first author (Yupu Li) is grateful to G. Briers for skillful assistance in TEM microscopy (microdiffraction and EDX), to R. Sweeney for his assistance in XRD measurements, and to N. Frost for his contribution to TEM sample preparation.


## References


1. X. X. XI, G. LINKER, O. MEYER, E. NOLD, B. OBST, F. RATZEL, R. SMITHEY, B. STREHLA, F. WESCHENFELDER and J. GEERK, *Z. Phys. B-Condensed Matter* **74** (1989) 13.
2. U. POPPE, J. SCHUBERT, R. R. ARONS, W. EVERS, C. H. FREIBURG, W. REICHERT, K. SCHMIDT, W. SYBERT and K. URBAN, *Solid State Communications* **66** (1988) 661.
3. U. POPPE, N. KLEIN, U. DAHNE, H. SOLTNER, C. L. JIA, B. KABIUS, K. URBAN, A. LUBIG, K. SCHMIDT, S. HENSEN, S. ORBACH, G. MULLER and H. PIEL, *J. Appl. Phys.* **71** (1992) 5572.
4. F. J. MULLER, J. C. GALLOP and A. D. CAPLIN, *Supercon. Sci. Tech.* **4** (1991) 616.
5. J. W. RADCLIFFE, L. F. COHEN, G. K. PERKINS, A. D. CAPLIN. T. J. TATE, M. J. LEE, F. M. SABA, P. QUINCEY, R. E. SOMEKH and P. PRZSLUPSKI *J. Alloys and Compounds* **195** (1993) 467.
6. YUPU LI, J. A. KILNER, T. J. TATE, M. J. LEE, F. M. SABA, L. F. COHEN, A. D. CAPLIN and P. G. QUINCEY, *J. Appl. Phys.* **75** (1994) 4081.
7. Y. H. LI, J. A. KILNER, YUPU LI, D. LACEY, A. D. CAPLIN and R. E. SOMEKH, *J. Mater. Sci.* **30** (1995) 3968.
8. YUPU LI, J. A. KILNER, T. J. TATE, M. J. LEE, Y. H. LI, R.E. SOMEKH and P. PRZYSLUPSKI, *J. Appl. Phys.* **78** (1995) 344.
9. YUPU LI, J. A. KILNER, T. J. TATE, M. J. LEE, F. M. SABA, L. F. COHEN, A. D. CAPLIN and P. G. QUINCEY, *Nucl. Instr. and Meth.* **B85** (1994) 281.
10. A. INAM, M. S. HEGDE, X. D. WU, T. VENKATESAN, P. ENGLAND, P. F. MICELI, E. W. CHASE, C. C. CHANG, J. M. TARASCON and J. B. WACHTMAN, *Appl. Phys. Lett.* **53** (1988) 908.
11. T. VENKATESAN, X. D. WU, R. MUENCHAUSEN and A. PIQUE, MRS Bulletin, Vol. XVII, No. 2, (1992) 55.
12. O. EIBL and B. ROAS, *J. Mater. Res.* **5** (1990) 2620.
13. Y. ZHU, M. SUENAGA, Y. XU, R. L. SABATINI and A. R. MOODENBAUGH, *Appl. Phys. Lett.* **54** (1989) 374.
14. Y, ZHU, M. SUENAGE and Y. XU, *J. Mater. Res.* **5** (1990) 1380.
15. S. IKEDA, K. KIMURA, A. MATSUSHITA, H. AOKI, T. HATANO, T. MATSUSHITA and K. OGAWA, *Mater. Res. Soc. Symp. Proc.* **99** (1988) 215.
16. T. K. WORTHINGTON, W. J. GALLAGHER, D. L. KAISER, F. H. HOLTZBERG and T. R. DINGER, *Physica C* **153–155** (1988) 32.
17. S. JIN, T. H. TIEFEL, R. C. SCERWOOD, M. E. DAVIS, R. B. VAN DOVER, G. W. KAMMLOTT, R. A. FASTNACHT and H. D. KEITH, *Appl. Phys. Lett.* **52** (1988) 2074.
18. Y. H. LI, C. LEACH and P. G. QUINCEY, *J. Mater. Sci. Lett.* **14** (1995) 670.
19. B. OH, K. CHAR, A. D. KENT, M. NAITO, M. R. BEASLEY, T. H. GEBALLE, R. H. HAMMOND, A. KAPITULNIK and J. M. GRAYBEAL, *Phys. Rev.* **B37** (1988) 7861.
20. YUPU LI, J. A. KILNER, T. J. TATE, M. J. LEE, Y. H. LI and P. G. QUINCEY, *Nucl. Instr. and Meth.* **B99** (1995) 627.
21. A. BARKATT, H. HOJAJI, R. W. AMARAKOON and J. G. FAGAN, MRS Bulletin XVII, No. 9 (1993) 45.
22. YUPU LI, J. A. KILNER, T. J. TATE, M. J. LEE, R. J. CHATER, H. FOX, R. A. DE. SOUZA and P. G. QUINCEY, *Phys. Rev.* **B51** (1995) 8498.
23. D. KUMAR, P. R. APTE, R. PINTO, M. SHARON and L. C. GUPTA *J. Electrochem. Soc.* **141** (1994) 1611.
24. M. P. SIEGAL, J. M. PHILLIPS, R. B. VAN DOVER, E. M. GYORGY, A. E. WHITE and J. H. MARSHALL, *Mat. Res. Soc. Symp. Proc.* **275** (1992) 293.
25. C. P. BEAN, *Rev. Mod. Phys.* **36** (1964) 31.



*Received 3 January 1996*
*and accepted 15 January 1996*